Diffusion properties of active particles with directional reversal

R Grossmann, Fernando Peruani, M Bär

Diffusion properties of active particles with directional reversal

R Großmann[1], F Peruani[2] and M Bär[1]

[1] Physikalisch-Technische Bundesanstalt Berlin, Abbestr. 2-12, 10587 Berlin, Germany

[2] Laboratoire J. A. Dieudonné, Université de Nice Sophia Antipolis, UMR 7351 CNRS, Parc Valrose, F-06108 Nice Cedex 02, France

E-mail: grossmann@physik.hu-berlin.de

Abstract. The diffusion properties of self-propelled particles which move at constant speed and, in addition, reverse their direction of motion repeatedly are investigated. The internal dynamics of particles triggering these reversal processes is modeled by a stochastic clock. The velocity correlation function as well as the mean squared displacement is investigated and, furthermore, a general expression for the diffusion coefficient for self-propelled particles with directional reversal is derived. Our analysis reveals the existence of an optimal, finite rotational noise amplitude which maximizes the diffusion coefficient. We comment on the relevance of these results with regard to microbiological systems and suggest further experiments in this context.

Submitted to: *New J. Phys.*

1. Introduction

Active matter systems – ensembles of self-driven particles – are a central subject of nonequilibrium statistical physics [1–4]: examples include micron-sized active colloids or rods driven by chemical reactions [5, 6] or by the Quincke effect [7, 8] as well as macroscopic collective motion patterns in bird flocks or sheep herds [9–11]. In particular, the study of bacterial systems as well as their theoretical analysis within simple self-propelled particle models has lead to interesting insights into the physics of active matter – consider, for example, the clustering of myxobacteria [12, 13] or the dynamic vortex formation in dense suspensions of swimming bacteria [14–16].

In order to understand the cooperative behavior of active particles as well as the associated pattern formation processes, reliable knowledge of the dynamics of individual entities is crucial. In this work, we therefore focus on the dynamics of individual active particles. We particularly consider particles that are able to reverse their direction of motion repeatedly. More precisely, particles follow an alternating motion pattern where rather persistent motion is interrupted by sudden reversals of the direction of motion.

This type of motion has been reported in a variety of bacterial systems [17–25]. For instance, the soil bacterium *Myxococcus xanthus* constitutes a paradigmatic example of a bacterium exhibiting periodic reversals in the direction of motion. *M. xanthus* is able to rebuild its internal structure such that the polarity of the motility engine switches repeatedly enabling alternating back and forth motion [17,18]. Under certain conditions, the reversals of several, densely packed bacteria appear synchronously leading to remarkable accordion wave patterns [26, 27]. Apart from myxobacteria, a variety of marine microorganisms exhibit "run & reverse" motion [19], such as *Pseudoalteromonas haloplanktis* and *Shewanella putrefaciens* [20]. Similar motion patterns were found in variety bacterial species, such as *Pseudomonas citronellolis* [28], *Paenibacillus dendritiformis* [21] and have also been reported for *Pseudomonas putida* [22–25].

More complex, three-step ("run-reverse-flick") motion patterns, composed of rather

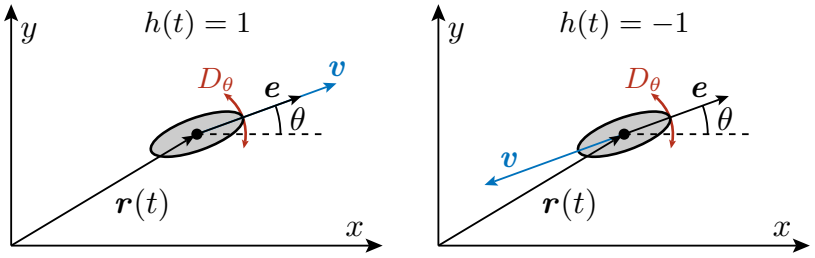

Figure 1. Schematic visualization of a particle at position $\boldsymbol{r}(t)$. Its body axis is oriented along the unit vector $\boldsymbol{e}$ (black arrow). *Left*: The motility engine is in state $h(t) = 1$; *right*: the propulsion engine is in the opposite state, $h(t) = -1$. The velocity of a particle, depicted by a blue arrow, is determined by $\boldsymbol{v}(t) = v_0\boldsymbol{e}(t)h(t)$. The red arrows indicate stochastic rotation of the body axis due to external inhomogeneities or fluctuations of the propelling engine modeled by white noise with intensity D_θ.

straight runs, directional reversals and 90° turns, were found in the marine bacterium *Vibrio alginolyticus* [29, 30]. In this context it has been speculated that bacteria can adopt their flip and reversal frequencies to the environmental conditions thus affecting their chemotactic response in order to detect and climb up chemical gradients more efficiently [29]. Similar questions were addressed theoretically within the context of self-propelled particle models. The chemotactic drift of self-propelled particles with run-reverse-flick motility was studied in [31]. the diffusion properties of active Brownian particles [2] with directional reversal in one spatial dimension were investigated in [32].

In this work, we study the diffusion properties of self-driven particles with directional reversal from a theoretical point of view. Generally, the microscopic dynamics of active particles results from the complex interplay of multiple factors: particle shape, detailed properties of the propulsion mechanism, interaction with the surroundings, e.g. hydrodynamic interaction with a fluid or friction on a surface, etc. Here, we abstain from modeling the details of the self-propulsion mechanism and reduce the complexity of the biochemical processes involved in the reversal events to a simple clock model as discussed in detail below. Our minimalistic approach to the problem consists of considering self-propelled particles such that:

(i) the propulsive force enabling a particle to move actively is counterbalanced by friction leading to active motion at a non-vanishing, constant, characteristic speed v_0;

(ii) the trajectories of particles are not perfectly straight lines due to fluctuations of the driving force or spatial heterogeneities, which is taken into account by the addition of rotational noise;

(iii) reversal events involve sudden transitions in the polarity of the moving direction of the particle, which aims at modeling the switching of the propelling engine between two states that correspond to "forward" and "backward" motion (for an illustration of the process see Fig. 1).

We exclusively consider homogeneous spatial environments without addressing questions related to chemotaxis.

This work is structured as follows. Section 2 introduces a paradigmatic model for the spatial dynamics of active particles with directional reversal. Moreover, central quantities of interest are defined and their interrelation is discussed. In particular, we derive a general expression for the diffusion coefficient of active particles with reversal. In section 3, we introduce a stochastic clock model representing the intracellular biochemical processes triggering reversal events. This simple model allows us to reproduce the characteristic shape of the distribution of times in between two consecutive reversal events as observed in experiments. We use this clock model to illustrate characteristic properties of the velocity correlation function, mean-squared displacement and the diffusion coefficient of active particles with reversal. In section 4, we extend the clock model describing the reversal dynamics by a renewal process. The analysis of this general model for reversing self-propelled particles reveals that – under certain

circumstances – the diffusion coefficient exhibits a maximum at a finite rotational noise intensity. This resonance effect is explained in detail and the relevance of this finding for bacterial systems is addressed by comparing theoretical predictions with (existing) experimental measurements. An outlook – accompanied by a summary of our main results – is given in the last section.

2. Active particles with reversal

2.1. Dynamics in general

In the following, we describe the mathematical model of self-propelled particles with directional reversal. Active particles, e.g. bacteria, exhibit a body axis, which we denote by an unit vector $\boldsymbol{e}(t)$ (see also Fig. 1). Suppose that the propulsion engine of a particle switches between two states in a cyclic manner allowing alternating parallel (forward) and antiparallel (backward) motion with respect to this axis‡. The two states of the internal motor are reflected by a state function $h(t) \in \{-1, 1\}$. A reversal event is then described by the transition

$$h(t) \;\rightarrow\; -h(t). \tag{2.1}$$

This process is assumed to be fast compared to the mean time in between two reversals as observed experimentally [17, 24]. The time between transitions is modeled by a clock model, which is defined in the next section.

The velocity $\boldsymbol{v}(t)$ of a particle is determined by the product of the characteristic speed v_0 – we assume a stationary force balance of driving and drag forces neglecting speed fluctuations –, the unit vector $\boldsymbol{e}(t)$ indicating the orientation of the body axis as well as the state of the propelling engine $h(t)$. Therefore, the spatial dynamics of a self-propelled particle with directional reversal reads

$$\frac{\mathrm{d}\boldsymbol{r}(t)}{\mathrm{d}t} = \boldsymbol{v}(t) = v_0 \boldsymbol{e}(t) h(t), \tag{2.2}$$

where $\boldsymbol{r}(t)$ hereafter denotes the position in space§.

We assume that the orientation of the body axis fluctuates stochastically due to spatial heterogeneities or noise associated to the self-propelling engine. This random reorientation is taken into account by addition of rotational diffusion. Here, we focus on the motion in two spatial dimensions, i.e. on substrates – the most relevant experimental setup. In two dimensions, the orientation of the body axis is determined by a time-dependent polar angle $\theta(t)$, cf. Fig. 1 for an illustration. The temporal dynamics of the

‡ Reversals of the internal polarity are, e.g., observed in colonies of gliding myxobacteria, where internal oscillations of the protein dynamics cause switches in cell polarity and, correspondingly, in the direction of motion of bacterial cells [33, 34].

§ This model equivalently describes particles which perform abrupt 180° turns instead of reversals. The function $h(t)$ is a bookkeeping parameter serving as a convenient description of turns in this case.

body axis, parametrized by the polar angle, reads

$$\boldsymbol{e}(t) = \begin{pmatrix} \cos\theta(t) \\ \sin\theta(t) \end{pmatrix}, \quad \frac{\mathrm{d}\theta(t)}{\mathrm{d}t} = \sqrt{2D_\theta}\,\xi(t). \tag{2.3}$$

The random process $\xi(t)$ denotes Gaussian white fluctuations with zero mean, $\langle \xi(t) \rangle = 0$, and temporal δ-correlations: $\langle \xi(t)\xi(t') \rangle = \delta(t-t')$.

The noise intensity D_θ is inversely proportional to the persistence length $l_p \sim v_0/D_\theta$ of the trajectory of an active particle. In general, D_θ itself may depend on additional parameters such as the speed itself [35]. However, we will treat it as an independent parameter in this context.

As discussed below, our results are not restricted to two dimensional systems since the motion of a self-propelled particle in two dimensions is not fundamentally different from corresponding three (or higher) dimensional cases [36]. We will comment in the respective paragraphs below which findings do quantitatively change in dimensions larger than two. Note that our analysis automatically contains the one-dimensional motion of self-propelled particles with directional reversal: the one dimensional back and forth motion along a line is recovered in the zero noise limit ($D_\theta = 0$) in our model.

2.2. Velocity correlation, mean-squared displacement and diffusion coefficient

In this section, we define several important observables used to characterize the motion pattern of self-propelled particles and briefly discuss their interrelation. A general expression for the diffusion coefficient of self-propelled particles with reversal is derived.

The central quantity of interest is the correlation function of the velocity:

$$\langle \boldsymbol{v}(t) \cdot \boldsymbol{v}(t') \rangle = v_0^2 \, \langle \boldsymbol{e}(t) \cdot \boldsymbol{e}(t') \rangle \, \langle h(t) h(t') \rangle \, . \tag{2.4}$$

In the expression above, we assumed the stochastic independence of the temporal dynamics of the body axis $\boldsymbol{e}(t)$ and the occurence of reversal events. This is a reasonable assumption since both processes are of different physical origin. Due to the stochastic independence, the calculation of the velocity correlation function can be done in two subsequent steps, considering the dynamics of the body axis and the reversal dynamics separately.

We point out that the correlation function of the body axis, $\langle \boldsymbol{e}(t) \cdot \boldsymbol{e}(t') \rangle$, is equal to the corresponding correlation function of a self-propelled particle without reversal. This limit is recovered from Eq. (2.4) by setting $h(t) = 1$ for all times. This correlation function is known to decay exponentially as discussed in [37, 38]:

$$\langle \boldsymbol{e}(t) \cdot \boldsymbol{e}(t') \rangle = e^{-D_\theta |t-t'|}. \tag{2.5}$$

Thus, the velocity correlation function reads

$$\langle \boldsymbol{v}(t) \cdot \boldsymbol{v}(t+\tau) \rangle = v_0^2 \, e^{-D_\theta \tau} C_{hh}(t,\tau), \tag{2.6}$$

where $\tau > 0$ and $C_{hh}(t,\tau) = \langle h(t) h(t+\tau) \rangle$. Due to the exponentially decaying envelope, the velocity correlation function does not possess heavy tails for any nonzero noise D_θ

excluding superdiffusion a priori irrespective of $C_{hh}(t,\tau)$. Subdiffusion is neither expected for finite noise amplitudes. Therefore, the mean squared displacement and, in particular, the diffusion coefficient are sufficient to characterize the long-term motion. Qualitatively, these arguments hold in higher spatial dimensions as well: In d spatial dimensions, the correlation functions decays according to $\langle \boldsymbol{e}(t)\cdot\boldsymbol{e}(t')\rangle = e^{-D_\varphi(d-1)|t-t'|}$. Thus, the correlation time is affected by the spatial dimensionality only. However, the qualitative exponential decay exists in all dimensions [36].

The mean squared displacement is directly related to the velocity correlation function via the following double integral, known as Taylor-Kubo formula [39, 40]

$$\left\langle |\boldsymbol{r}(t)-\boldsymbol{r}(0)|^2 \right\rangle = 2\int_0^t \mathrm{d}t' \int_0^{t'} \mathrm{d}t''\, \langle \boldsymbol{v}(t')\cdot\boldsymbol{v}(t'')\rangle, \tag{2.7}$$

which is proved by direct integration of Eq. (2.2) and using the symmetry of the velocity correlation function with respect to permutation of the times t' and t''. The asymptotic spatial diffusion coefficient $\mathcal{D}$ follows, in turn, from the mean squared displacement via

$$\mathcal{D} = \frac{1}{4}\cdot\lim_{t\to\infty}\left[\frac{\mathrm{d}\left\langle |\boldsymbol{r}(t)-\boldsymbol{r}(0)|^2\right\rangle}{\mathrm{d}t}\right]. \tag{2.8}$$

This definition can be rewritten by making use of the Taylor-Kubo relation. Subsequent insertion of the velocity correlation function, Eq. (2.6), finally yields

$$\mathcal{D} = \frac{v_0^2}{2}\cdot\int_0^\infty \mathrm{d}\tau\, e^{-D_\theta\tau}\lim_{t\to\infty}\Big[C_{hh}(t-\tau,\tau)\Big]. \tag{2.9}$$

We denote the correlation function in the limit $t\to\infty$ by

$$C_{hh}^{(eq)}(\tau) = \lim_{t\to\infty}\Big[C_{hh}(t-\tau,\tau)\Big]. \tag{2.10}$$

Consequently, the diffusion coefficient is determined by the integral transform

$$\mathcal{D} = \frac{v_0^2}{2}\int_0^\infty \mathrm{d}\tau\, e^{-D_\theta\tau}\, C_{hh}^{(eq)}(\tau) = \frac{v_0^2}{2}\,\widehat{C}_{hh}^{(eq)}(D_\theta). \tag{2.11}$$

Interestingly, the integral in Eq. (2.11) is structurally equivalent to the Laplace transform‖ of the correlation function $C_{hh}^{(eq)}(\tau)$. This central result is convenient for the calculation of the diffusion coefficient because the correlation function of the process $h(t)$ can be calculated in the Laplace domain whereas the inverse transformation is often impossible.

We conclude this section by giving the diffusion coefficient for self-propelled particles in spatial dimensions $d\geq 2$ which is similar in structure to the two dimensional result:

$$\mathcal{D} = \frac{v_0^2}{d}\,\widehat{C}_{hh}^{(eq)}\Big(D_\theta(d-1)\Big). \tag{2.12}$$

Thus we obtain the concise result that the diffusion coefficient of a self-propelled particle with directional reversal is determined by the Laplace transform of the correlation function of the reversal process $h(t)$.

‖ We use the definition $\widehat{f}(s)=\int_0^\infty \mathrm{d}t\, e^{-st} f(t)$ for the Laplace transform $\widehat{f}(s)$ of a function $f(t)$ [41].

3. A clock model

3.1. Directional reversal controlled by an intracellular clock

The triggering of reversal events is controlled by complex processes taking place inside a particle giving rise to stochastic occurrences of reversals. Here, we do not model the internal particle dynamics in detail since these processes are hardly accessible experimentally anyway. We rather employ a coarse-grained description capturing the essential phenomenology of the reversal dynamics.

In order to trigger a single reversal, a certain number of biochemical (activation) processes needs to be executed. Following this reasoning, we propose a *stochastic clock model* (cf. Fig. 2) which is intended to represent the internal particle dynamics. Suppose that each of the activation processes – corresponding to ticks of the clock – arises at a given rate which we assume to be all identical for simplicity. Whenever the watch hand completes a full revolution, i.e. M consecutive ticks appeared, a reversal event is triggered.

We model the ticking of the clock as a stochastic process: the watch hand ticks with a probability $\kappa\Delta t$ in a small time increment Δt. Thus, the ticking of the clock is described, mathematically speaking, by Poisson a process [42] with rate κ. This stochastic process is unique since, as has already been mentioned, the probability that a tick is observed in a given time interval is constant and, hence, independent of the process history.

Whereas the biochemical processes controlling the reversals are not directly observable, the resulting distribution of the times elapsed in between two successive reversal events – usually called *run-time distribution* – is easily accessible experimentally.

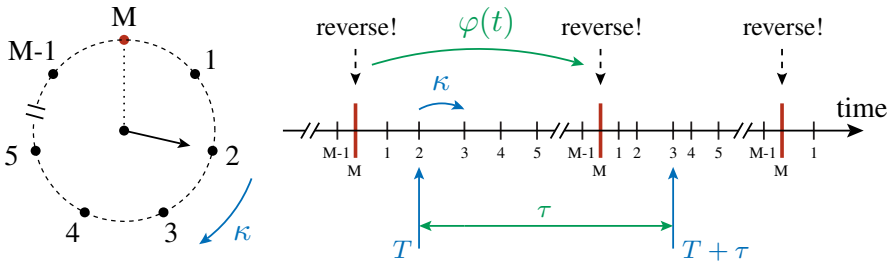

Figure 2. Schematic visualization of the internal particle dynamics modeled by a stochastic clock with M ticks. The black arrow indicates the clock hand which jumps in a small time interval Δt with probability $\kappa\Delta t$. Thus, the ticking of the clock is a Poisson process with rate κ. Whenever the clock hand crosses the state M, marked in red, a reversal process is triggered. The timeline on the right symbolizes the same process as a function of time. The time intervals in between two reversal events are distributed according to the probability density $\varphi(t)$, Eq. (3.1). Furthermore, we indicate the state of the clock at a time T (state 2). After a time τ, a reversal may have occurred (in Fig.: one reversal) and the clock is in another internal state (in Fig.: state 3).

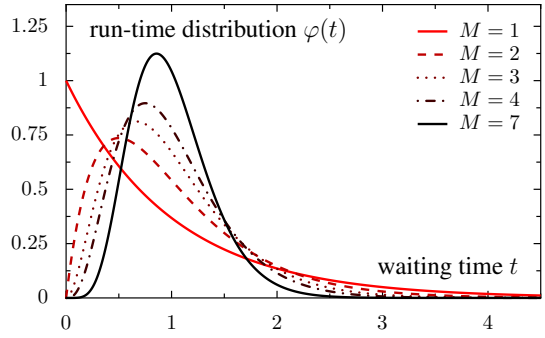

Figure 3. Run-time distribution (3.1) resulting from the clock model for several values of M (# ticks of the clock). The run-time distribution reduces to an exponential distribution for $M = 1$. In contrast, $\varphi(t)$ tends towards a Gaussian bell-shape for large values of M. The rate $\kappa = M$ was adjusted such that the mean of $\varphi(t)$ equals one: $\langle t \rangle = \int_0^\infty \mathrm{d}t\, t\, \varphi(t) \stackrel{!}{=} 1$.

We will denote the run-time distribution by $\varphi(t)$. The clock model introduced above implies one particular run-time distribution (γ-distribution) which reads

$$\varphi(t) = \frac{\kappa^M t^{M-1} e^{-\kappa t}}{(M-1)!}. \tag{3.1}$$

Naturally, $\varphi(t)$ depends on two parameters: the number of ticks M of the clock as well as the rate κ at which ticks of the watch hand are observed. The distribution is plotted for several values of M in Fig. 3. The limiting case $M = 1$ is special since the clock possesses only one tick, such that every tick of the clock implies a reversal event. Accordingly, the occurrence of reversals is a Poisson process and $\varphi(t)$ is an exponential distribution in this case. In contrast, an asymmetric bell shape is observed for $M > 1$. In the limit of large M, $\varphi(t)$ tends towards a Gaussian distribution. We comment on the applicability of the run-time distribution $\varphi(t)$ in section 5 by a direct comparison to experimentally observed distributions.

The most important characteristics of the run-time distribution are its mean $\langle t \rangle$ determining the average frequency $\lambda_r = 1/\langle t \rangle$ at which reversal events are observed as well as its width $\sigma^2 = \left\langle (t - \langle t \rangle)^2 \right\rangle$. The mean time separating two reversal events is equal to the M-fold of the mean waiting time for a single tick on the clock determined by κ^{-1}. Therefore, the reversal frequency is given by $\lambda_r = \kappa/M$. The variance σ^2 of the gamma distribution, Eq. (3.1), reads $\sigma^2 = M/\kappa^2$. Hence, the coefficient of variation c_v, i.e. the standard deviation over the mean, decreases with the number of intermediate steps: $c_v = 1/\sqrt{M}$. Consequently, the interpretation of the parameters of the clock model is straightforward: the accuracy of the clock, i.e. the regularity at which reversal events occur – reflected by the width of the run-time distribution $\varphi(t)$ – is determined by the number of ticks M, whereas the ticking rate κ is directly proportional to the mean reversal frequency λ_r.

3.2. Analysis of the clock model

Starting from the clock model, the calculation of the correlation function $C_{hh}(t,\tau)$ is sketched. Subsequently, the resulting phenomenology of this clock model is discussed.

The reversal process $h(t)$ which determines the state of the propelling engine of a particle does only take two values corresponding to "forward" and "backward" motion: $h(t) \in \{-1, 1\}$. Therefore, the product $h(t) \cdot h(t+\tau)$ is equal to plus or minus one depending on the number of reversal events in the time window τ beginning at time t. Accordingly, we can calculate the correlation function $C_{hh}(t,\tau) = \langle h(t)h(t+\tau)\rangle$ of the process $h(t)$ via

$$C_{hh}(t,\tau) = \langle h(t)h(t+\tau)\rangle = \sum_{N=0}^{\infty}(-1)^N P_N(t,\tau), \tag{3.2}$$

where $P_N(t,\tau)$ denotes the probability that exactly N reversals occurred within the time interval τ.

The clock model yields an illustrative way to calculate the probabilities $P_N(t,\tau)$, cf. Fig. 2 for a visualization. We make use of the fact that the ticking of the clock is equivalent to a Poisson process with rate κ. For a Poisson process, the probability $\psi_n(t)$ to observe n ticks of the clock in a given time interval of length t is determined by

$$\frac{\mathrm{d}\psi_n(t)}{\mathrm{d}t} = \begin{cases} -\kappa\psi_0(t), & n = 0, \\ -\kappa\psi_n(t) + \kappa\psi_{n-1}(t), & n \geq 1, \end{cases} \tag{3.3}$$

whose solution is found by successive integration:

$$\psi_n(t) = \frac{(\kappa t)^n e^{-\kappa t}}{n!}. \tag{3.4}$$

Using this result, the probability to observe no reversal within a time interval of length τ beginning at t can be written as

$$P_0(t,\tau) = \underbrace{\sum_{N=0}^{\infty}\sum_{n=0}^{M-1}\psi_{NM+n}(t)}_{(a)}\underbrace{\sum_{m=0}^{M-n-1}\psi_m(\tau)}_{(b)}. \tag{3.5}$$

This equation consist of two parts to be interpreted as follows. The terms (a) reflect the state of the clock at time t. The clock is in one of the M internal states, denoted by n. Previous to time t, a certain number of reversals N have already occurred. Thus, $NM + n$ ticks of the clock were observed up to time t in total. However, the number of reversals and the state of the internal clock are not relevant – that is why N and n is to be summed over. The third sum, abbreviated by (b) in Eq. (3.5), reflects the probability that m additional ticks of the clock are observed. The set of m values is constrained to those values satisfying $n+m < M$, i.e. such that no reversal event occurs within the time interval τ. Pictorially speaking, this is fulfilled if the watch hand does not complete a revolution within τ (see left of Fig. 2).

Along similar lines of arguments, the probability to observe k reversals within time τ can be derived:

$$P_k(t,\tau) = \sum_{N=0}^{\infty} \sum_{n=0}^{M-1} \psi_{NM+n}(t) \sum_{m=0}^{M-1} \psi_{Mk+m-n}(\tau). \tag{3.6}$$

Apparently, the first part does not change whereas the third sum is replaced by the probabilities that exactly k reversals occur within τ corresponding to k revolutions of the watch hand.

Eqs. (3.2)–(3.6) allow the calculation of the correlation function by performing the summations. In time domain, this is not possible in general. However, the summation can be done in a closed form in Laplace domain by inserting the Laplace transform of $\psi_n(t)$,

$$\widehat{\psi}_n(s) = \frac{\kappa^n}{(\kappa+s)^{n+1}}, \tag{3.7}$$

and summing several geometrical series. The probabilities P_0 and P_k read in Laplace space as follows:

$$\widehat{\widehat{P}}_0(s,u) = \frac{1}{u} \cdot \left[\frac{1}{s} - \frac{1}{1-\widehat{\varphi}(s)} \cdot \frac{\widehat{\varphi}(s) - \widehat{\varphi}(u)}{u-s} \right], \tag{3.8a}$$

$$\widehat{\widehat{P}}_k(s,u) = \frac{1-\widehat{\varphi}(u)}{u} \cdot \frac{[\widehat{\varphi}(u)]^{k-1}}{1-\widehat{\varphi}(s)} \cdot \frac{\widehat{\varphi}(s) - \widehat{\varphi}(u)}{u-s}. \tag{3.8b}$$

Finally, we also obtain a closed expression for the correlation function:

$$\widehat{\widehat{C}}_{hh}(s,u) = \frac{1}{u} \cdot \left[\frac{1}{s} - \frac{2}{u-s} \cdot \frac{\widehat{\varphi}(s) - \widehat{\varphi}(u)}{[1+\widehat{\varphi}(u)] \cdot [1-\widehat{\varphi}(s)]} \right]. \tag{3.9}$$

In Eq. (3.8) and (3.9), the Laplace transform

$$\widehat{\varphi}(s) = \left[\frac{\kappa}{\kappa+s} \right]^M \tag{3.10}$$

of the run-time distribution $\varphi(t)$, cf. Eq. (3.1), was identified and abbreviated for convenience.

In general, the correlation function depends on both, t and τ, via s and u in Laplace domain – the reversal dynamics $h(t)$ possesses memory reflecting the non-Markovian [42] character of the dynamics. For the long-time diffusion properties, however, only the limiting behavior $\lim_{t\to\infty} \left[C_{hh}(t,\tau) \right] = C_{hh}^{(eq)}(\tau)$ is relevant. The Laplace transform of $C_{hh}^{(eq)}(\tau)$ is found from the general solution, Eq. (3.9), as follows [41]:

$$\widehat{C}_{hh}^{(eq)}(u) = \lim_{t\to\infty} \left[\widehat{C}_{hh}(t,u) \right] = \lim_{s\to 0} \left[s\, \widehat{\widehat{C}}_{hh}(s,u) \right] \tag{3.11a}$$

$$= \frac{1}{u} \cdot \left[1 - \frac{2\lambda_r}{u} \cdot \frac{1-\widehat{\varphi}(u)}{1+\widehat{\varphi}(u)} \right]. \tag{3.11b}$$

Consequently, the central quantity of interest, the correlation function $C_{hh}^{(eq)}(\tau)$ determining the diffusion properties of an active particle whose reversal is triggered by an internal clock, is known.

3.3. Results: illustration of the clock model

In the following, we illustrate our results and outline their implications. We begin the discussion of the motion characteristics by recalling the general form of the velocity correlation function:

$$\langle \boldsymbol{v}(t) \cdot \boldsymbol{v}(t+\tau) \rangle = v_0^2 \, e^{-D_\theta \tau} C_{hh}(t,\tau). \tag{3.12}$$

For the self-propelled particle model considered here, the velocity correlation increases proportional to the squared speed. The rotational noise inducing a stochastic rotation of the body axis implies an exponential damping of the velocity correlations. The characteristic damping time τ_θ is inversely proportional to the amplitude of rotational fluctuations: $\tau_\theta = 1/D_\theta$. Accordingly, reversal events do only play an important role if the mean time $\langle t \rangle$ separating subsequent reversal events is smaller than or comparable to the correlation time τ_θ. In the opposite case, rotational noise causes the body axis to rotate within a shorter time compared to $\langle t \rangle$ implying the decorrelation of velocities within this time. To be concrete, let us suppose that reversal events occur at times t_1 and t_2. If the velocities $\boldsymbol{v}(t_1)$ and $\boldsymbol{v}(t_2-\epsilon)$, i.e. immediately before the next reversal event ($\epsilon \ll 1$), had already been uncorrelated, the reversal at time t_2 does not influence the velocity statistics. Consequently, diffusion properties are independent of the directional reversals in this regime.

The velocity correlation function is proportional to the correlation function of the reversal process $h(t)$ which was calculated in the preceding section for the clock model. The correlation function crucially depends on the number of ticks M of the clock. In Tab. 1, we summarize the correlation function $C_{hh}^{(eq)}(\tau)$ for the lowest M values which are also graphically shown in Fig. 4. For $M = 1$, the reversal process reduces to a Poisson process since every tick of the clock triggers a reversal event which therefore occur at a constant rate κ. Accordingly, the correlation function is exponentially decaying with a characteristic time determined by $1/\kappa$. More interesting behavior is observed if the clock possesses several ticks, $M \geq 2$: the correlation function does oscillate. Oscillations become more and more pronounced with increasing M. Remember that the number of ticks of the clock controls the accuracy of reversal event occurrences. In the limit $M \to \infty$, reversals would occur deterministically every $\langle t \rangle = 1/\lambda_r$ seconds implying a square wave signal form of the correlation function $C_{hh}^{(eq)}(\tau)$.

Table 1. Correlation functions $C_{hh}^{(eq)}(\tau)$ for the clock model.

number of ticks	correlation function
$M = 1$:	$C_{hh}^{(eq)}(\tau) = e^{-2\kappa\tau}$
$M = 2$:	$C_{hh}^{(eq)}(\tau) = e^{-\kappa\tau}\cos(\kappa\tau)$
$M = 3$:	$C_{hh}^{(eq)}(\tau) = \frac{1}{9}\left[e^{-2\kappa\tau} + 8e^{-\frac{\kappa\tau}{2}}\cos\left(\frac{\sqrt{3}\kappa\tau}{2}\right)\right]$
$M = 4$:	$C_{hh}^{(eq)}(\tau) = e^{-\kappa\tau}\cos\left(\frac{\kappa\tau}{\sqrt{2}}\right)\left[\cosh\left(\frac{\kappa\tau}{\sqrt{2}}\right) + \frac{1}{\sqrt{2}}\sinh\left(\frac{\kappa\tau}{\sqrt{2}}\right)\right]$

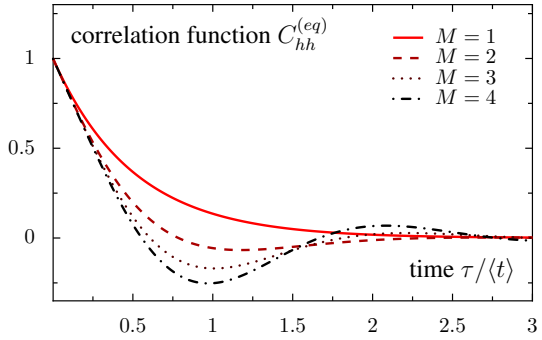

Figure 4. Correlation function $C_{hh}^{(eq)}(\tau)$, cf. Tab. 1, as a function of time τ for the clock model. The number of ticks of the clock is denoted by M. For $M \geq 2$, oscillations of the correlation function are observed. The limit $M = 1$ is special since the reversal process reduces to a Poisson process in this case. That is why correlations decay exponentially for $M = 1$.

Oscillations are likewise expected for the velocity correlation function, Eq. (3.12), in the low noise regime ($D_\theta \lesssim \lambda_r$) where oscillations reflect the recurrent back and forth motion of particles.

The existence of oscillatory velocity correlations is crucial for the properties of the mean squared displacement which can show oscillatory behavior as well. Typical time dependencies of the mean squared displacement in different regimes are shown in Fig. 5. The knowledge about the existence of (weakly) oscillating mean squared displacements is important for the analysis of experimental data. Real-world data are not expected to

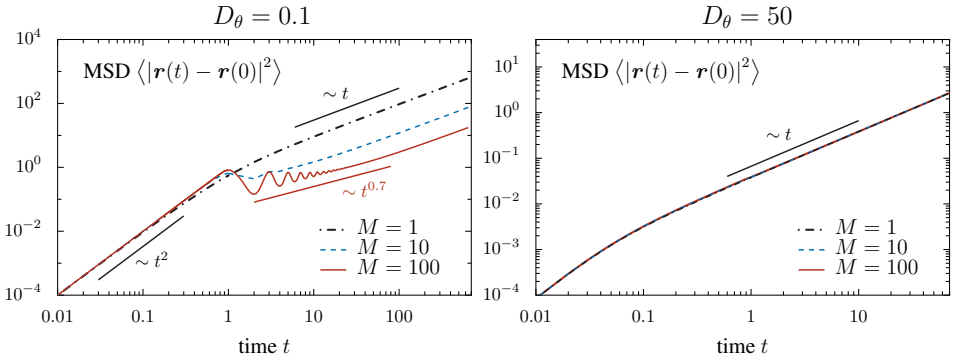

Figure 5. Mean squared displacement for several values of M: low noise regime (*left*) and high noise (*right*). In the low noise regime ($D_\theta < \lambda_r$), the mean squared displacement (MSD) shows oscillatory behavior for large M. In contrast, the reversal dynamics does not influence the diffusion properties for $D_\theta > \lambda_r$ (see main text for an explanation). Parameters were adjusted such that the reversal frequency $\lambda_r = 1$ in all cases: $\kappa = M$, $v_0 = 1$. The straight red line on the left indicates intermediate sublinear scaling due to oscillatory behavior of the MSD which could erroneously be interpreted as subdiffusion if oscillations are not properly resolved in an experiment. We emphazise, however, that the MSD increases *always linearly* in the long-time limit in our model.

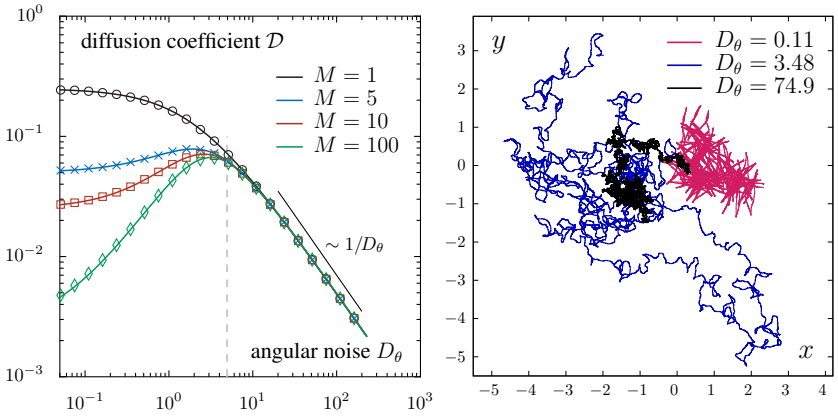

Figure 6. *Left*: Diffusion coefficient $\mathcal{D}$ as a function of the angular noise intensity D_θ from theory (3.13) shown by lines as well as numerical Langevin simulation (symbols). The light gray (dashed) line indicates the estimate for the optimal noise strength from a comparison of relevant timescales (cf. section 4.2). *Right*: Trajectories for three noise intensities D_θ. The diffusivity is maximal for an intermediate value D_θ (blue trajectory). Parameters: $v_0 = 1$, $\kappa = M$, $\lambda_r = 1$, numerical time step $\Delta t = 10^{-3}$. On the right: $M = 100$.

show oscillations as clean as the theoretical results discussed here. As a result, the mean squared displacement may misleadingly suggest a subdiffusive regime due to the visual impression from noisy data (see red line on the left of Fig. 5). We emphasize, however, that our model does not predict subdiffusion but normal diffusion in the long-time limit.

Since normal diffusion is expected, the motion is properly characterized by the spatial diffusion coefficient $\mathcal{D}$. Due to the preparatory work done in previous sections, its derivation is straightforward. The diffusion coefficient is obtained from the general solution, Eq. (2.11), by inserting the Laplace transform of the correlation function of the reversal dynamics, Eq. (3.11*b*). For the clock model, we obtain the diffusion coefficient

$$\mathcal{D} = \frac{v_0^2}{2D_\theta} \cdot \left[1 - \frac{2\kappa}{D_\theta M} \cdot \frac{(\kappa + D_\theta)^M - \kappa^M}{(\kappa + D_\theta)^M + \kappa^M} \right]. \tag{3.13}$$

In Fig. 6, the diffusion coefficient as a function of the angular noise is shown for several values of M. The analysis reveals that a finite, optimal noise value D_θ exists which maximizes the diffusion coefficient. The existence of this maximum can intuitively be understood by looking at trajectories of particles in the different regimes, as shown in Fig. 6 on the right. For low noise ($D_\theta \ll \lambda_r$), the particle moves back and forth along a line due to reversal. If, in addition, reversals occur in a fairly regular fashion, the trajectories are typically rather localized and the diffusivity is low. On the other hand, the diffusion coefficient is likewise low for high angular noise ($D_\theta \gg \lambda_r$) since particles perform a lot of turns thus preventing the departure from the initial position. Hence, the diffusivity is maximal for intermediate amplitudes of the rotational noise. The physics of this resonance effect is addressed in detail in the following section.

4. Generalization – reversal events as renewal process

In the previous section, we introduced an extension of a self-propelled particle model by including recurrent reversals of the direction of motion. The internal particle dynamics was modeled by a clock representing the activation of certain biochemical processes that in turn trigger reversals events. Since the "ticking" of the clock was assumed to be a stochastic process, subsequent reversals occur after stochastic waiting times. By construction, these waiting times are independent and identically distributed according to the run-time distribution $\varphi(t)$. Mathematically, this constitutes the definition of a renewal process [43] – more precisely, the transition times determining the reversal dynamics $h(t)$ are controlled by a renewal process uniquely defined by a waiting time probability density function $\varphi(t)$.

In this section, we discuss general diffusion properties of self-propelled particles with directional reversal making use of the analogy to renewal theory. We relax the assumption that the run-time distribution $\varphi(t)$ is determined by the clock model thus considering arbitrary run-time distributions which may either be derived from more detailed models or measured experimentally.

Previously, it was argued that the central object of interest is the correlation function of the reversal process: $C_{hh}(t,\tau) = \langle h(t)h(t+\tau)\rangle$. This correlation function $C_{hh}(t,\tau)$ can be determined in Laplace domain without specification of the run-time distribution by using properties of renewal processes [44]. The derivation is based on similar ideas as the calculation presented in the context of the clock model (section 3.2). It turns out that Eq. (3.9),

$$\widehat{\widehat{C}}_{hh}(s,u) = \frac{1}{u}\cdot\left[\frac{1}{s} - \frac{2}{u-s}\cdot\frac{\widehat{\varphi}(s)-\widehat{\varphi}(u)}{[1+\widehat{\varphi}(u)]\cdot[1-\widehat{\varphi}(s)]}\right], \tag{4.1}$$

as well as the corresponding function in the long-time limit, Eq. (3.11),

$$\widehat{C}^{(eq)}_{hh}(u) = \frac{1}{u}\cdot\left[1 - \frac{2\lambda_r}{u}\cdot\frac{1-\widehat{\varphi}(u)}{1+\widehat{\varphi}(u)}\right], \tag{4.2}$$

constitute the correlation function for arbitrary run-time distributions (see e.g. [44] for a proof). Accordingly, the Laplace transform $\widehat{\varphi}(s)$ of the run-time distribution $\varphi(t)$ determines the correlation function of the reversal process. The inverse Laplace transformation in both arguments can be done analytically in special cases only. Note, however, that this transformation is not needed for the calculation of the diffusion coefficient via Eq. (2.12).

4.1. Diffusion coefficient

In section 2.2, we derived a simple formula for the diffusion coefficient: it is straightforwardly obtained from the Laplace transform of the correlation function $C^{(eq)}_{hh}(\tau)$, Eq. (4.2), by replacing the variable u by the noise amplitude D_θ:

$$\mathcal{D} = \frac{v_0^2}{2D_\theta}\cdot\left[1 - \frac{2\lambda_r}{D_\theta}\cdot\frac{1-\widehat{\varphi}(D_\theta)}{1+\widehat{\varphi}(D_\theta)}\right]. \tag{4.3}$$

This solution determines the diffusion coefficient for any run-time distribution $\varphi(t)$. Once $\varphi(t)$ has been derived from theoretical considerations – as it was done in the context of the clock model – or it was fitted to experimental data, the diffusion coefficient can immediately be calculated.

In the following, we discuss the properties of this solution. First, we note that the diffusion coefficient of a self-propelled particle with reversal is always lower compared to a particle which does never reverse its direction of motion if the trajectories are comparably persistent, i.e. if D_θ is equal in both cases. This can be seen from the fact that the term in brackets is always smaller than one since $\widehat{\varphi}(D_\theta) \in (0,1)$ for all $D_\theta > 0$:

$$\mathcal{D} = \frac{v_0^2}{2D_\theta} \cdot \left[1 - \frac{2\lambda_r}{D_\theta} \cdot \frac{1-\widehat{\varphi}(D_\theta)}{1+\widehat{\varphi}(D_\theta)}\right] < \frac{v_0^2}{2D_\theta}. \tag{4.4}$$

Henceforth, we discuss two limiting cases, namely the high noise limit ($D_\theta \gg \lambda_r$) and the low noise regime ($D_\theta \ll \lambda_r$). In the former case, we exploit that the Laplace transform of the waiting time distribution tends to zero for large values of its argument. Therefore, we obtain

$$\mathcal{D} \sim \frac{v_0^2}{2D_\theta} \cdot \left[1 - \mathcal{O}\left(\frac{\lambda_r}{D_\theta}\right)\right]. \tag{4.5}$$

Hence, the diffusion coefficient coincides with the diffusion coefficient of non-reversing self-propelled particles [37, 38]. This is plausible since reversals are not expected to influence the diffusion properties in the high noise regime as argued before in the context of the velocity correlation function, cf. Eq. (3.12).

We derive the low noise limit by expanding $\widehat{\varphi}(D_\theta)$ in a Taylor series:

$$\widehat{\varphi}(D_\theta) = \sum_{n=0}^{\infty} \frac{(-1)^n D_\theta^n}{n!} \int_0^\infty \mathrm{d}t\, t^n\, \varphi(t). \tag{4.6}$$

The series coefficients are determined by the moments¶ of the waiting time distribution $\varphi(t)$. However, it is more insightful to work with the central moments $\langle (\Delta t)^n \rangle = \int_0^\infty \mathrm{d}t\ (t - \langle t \rangle)^n \varphi(t)$. The diffusion coefficient is obtained by inserting this series into Eq. (4.3) and expanding the resulting expression in powers of the noise:

$$\mathcal{D} = \frac{\lambda_r v_0^2}{4} \left[\left\langle (\Delta t)^2 \right\rangle + \frac{1 - 2\lambda_r^3 \left\langle (\Delta t)^3 \right\rangle}{6} \cdot \frac{D_\theta}{\lambda_r^3} + \mathcal{O}\left(\frac{D_\theta^2}{\lambda_r^4}\right)\right]. \tag{4.7}$$

Interestingly, the diffusion coefficient is determined by the variance of the waiting time distribution for low noise values. Thus, the diffusion coefficient tends to zero for small noise amplitudes, if the reversal time distribution is narrow. Moreover, if the first Taylor coefficient is positive, i.e.

$$2\lambda_r^3 \left\langle (\Delta t)^3 \right\rangle < 1, \tag{4.8}$$

the diffusion coefficient *increases* proportional to the noise strength. Since the dependence of the diffusion coefficient on the noise is continuous and the diffusion coefficient decreases for large noise values, there must exist a maximum in between: an

¶ Here, we assume that the moments exist and are finite.

optimal angular noise value maximizes the diffusivity. Eq. (4.8) constitutes a sufficient condition for the existence of a maximum.

4.2. Resonance - optimal noise maximizes diffusion

The resonance effect – the maximization of the diffusion coefficient for a finite angular noise intensity – is understood by comparing the relevant timescales. For an illustration of the following arguments, see Fig. 7 and Fig. 8.

We give an intuitive argument why this maximum exists and estimate its position by rephrasing the problem as follows: *Suppose, a particle reverses its direction of motion every λ_r^{-1} seconds. How large should the angular noise strength D_θ be in order to maximize the diffusivity?* To answer this question, we note first that a self-propelled particle moves ballistically into the direction determined by $\boldsymbol{e}(t)$, i.e. it moves ballistically away from its initial position at small timescales. However, angular fluctuations cause the orientation of the body axis $\boldsymbol{e}(t)$ to rotate. Apparently, the particle tends to move back to its initial position if $\boldsymbol{e}(t)$ points into the opposite direction with respect to $\boldsymbol{e}(t_0)$. Thus, a particle could move further away from its initial position, if it reverses its direction of motion in this very moment. Hence, two relevant timescales exist: (i) the mean time between two reversal events and (ii) the characteristic time it takes for the body axis to rotate by approximately 180° driven by rotational noise. The former is determined by the inverse reversal frequency λ_r^{-1}. In order to estimate the latter, we note that the dynamics of the angle θ is equivalent to Brownian motion with diffusion coefficient D_θ in one dimension thus constituting a mean first-passage time problem: *What is the mean time $\tilde{\tau}$ it takes for a Brownian particle with diffusivity D_θ to escape out of the interval $(\theta_0 - \pi, \theta_0 + \pi)$, given that the initial position was θ_0?* The solution of the first-passage time problem yields the well known diffusion law: $\pi^2 = 2D_\theta\tilde{\tau}$. The comparison of both timescales, $\tilde{\tau} \stackrel{!}{=} \lambda_r^{-1}$, may be used to estimate the optimal noise

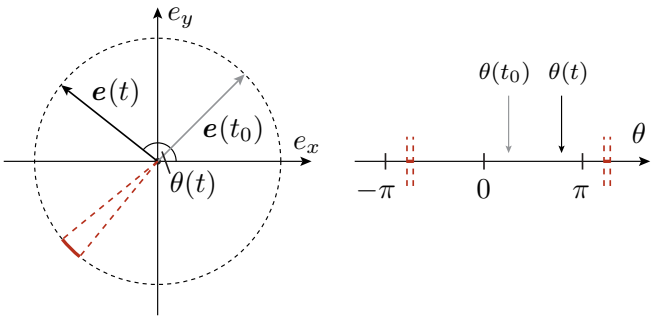

Figure 7. *Left*: Sketch of the temporal dynamics of $\boldsymbol{e}(t)$ determining the direction of motion of a particle. The red cone indicates a region where $\boldsymbol{e}(t)$ points in the opposite direction with respect to the initial direction of motion $\boldsymbol{e}(t_0)$. *Right*: The angles θ corresponding to the vectors shown on the left.

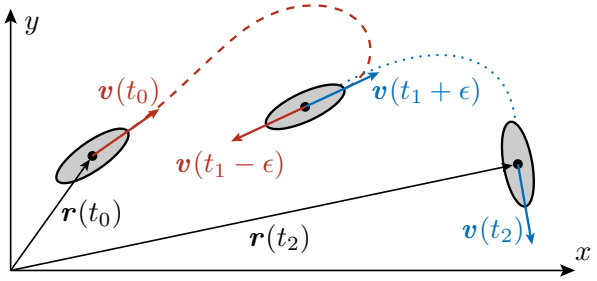

Figure 8. Illustration of the motion strategy for a maximal diffusion coefficient. A particle, initially located at $\boldsymbol{r}(t_0)$, reverses its direction at time t_1. If the velocity vector prior to the reversal event $\boldsymbol{v}(t_1-\epsilon)$, where $\epsilon \ll 1$, is antiparallel to the velocity at time t_0, the reversal will increase the probability that the particle departs from its initial position instead of moving back to the origin thus enhancing the diffusivity.

value:

$$\bar{D}_\theta \approx \frac{\lambda_r \pi^2}{2}\,. \tag{4.9}$$

This reasoning is valid if the first-passage time distribution as well as the reversal time distribution are sufficiently narrow. However, we obtain a rather reasonable estimate for the optimal noise amplitude as shown by the gray dashed line in Fig. 6.

5. Summary & outlook

In this work, we studied the diffusion properties of self-propelled particles that repeatedly reverse their direction of motion. We adopted a coarse-grained viewpoint aiming at describing the reversal dynamics phenomenologically and discussing the effects of the directional reversal on the diffusion properties of active particles within the framework of stochastic processes. For this purpose, we model individual particles as point-like objects with a propelling engine allowing for active motion at constant speed. Fluctuations of the driving motor as well as external heterogeneities are taken into account by addition of rotational noise. The internal dynamics of the propelling engine that controls reversal events is modeled by a simple clock model, where the ticks of the clock represent biochemical activation processes. We derived results for velocity correlation functions, mean squared displacement and, in particular, the diffusion coefficient for this model. Notably, we found that the mean squared displacement can show oscillatory behavior for intermediate times. Therefore, real-world experimental data must be analyzed carefully because the visual impression of noisy data may wrongly be interpreted as a subdiffusive regime if oscillations are not properly resolved.

In the second part, we generalized the results obtained from the clock model describing the reversal dynamics as a renewal process: subsequent reversal events occur after random waiting times which are distributed according to a given run-time distribution. Given a run-time distribution, we derived a general formula for the diffusion coefficient. Our analysis reveals that an optimal rotational noise value

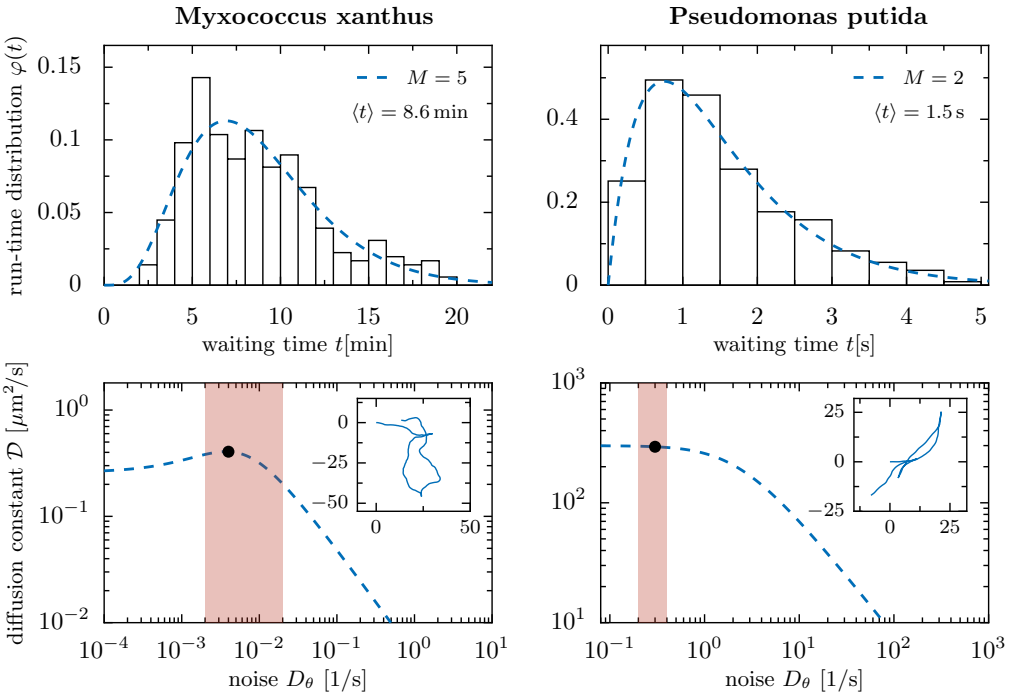

Figure 9. *Upper panel*: run-time distribution $\varphi(t)$ for the bacteria *Myxococcus xanthus* (left) and *Pseudomonas putida* (right). Experimentally observed distributions of myxobacteria and *Pseudomonas putida* – reproduced from [17] and [24], respectively – are represented by bars in the two upper panels. The lines represent the corresponding waiting time distributions from the clock model, Eq. (3.1), where parameters were estimated from the data according to Eq. (5.1).
Lower panel: diffusion coefficient $\mathcal{D}$ as predicted by the clock model, Eq. (3.13). We used the following estimates for the mean time in between two reversals obtained from the distributions above: $\langle t \rangle = 8.6\,\mathrm{min}$ and $\langle t \rangle = 1.5\,\mathrm{s}$, respectively. A characteristic speed was estimated to be $v_0 \approx 0.1\,\mu\mathrm{m/s}$ for myxobacteria [45] and $v_0 \approx 40\,\mu\mathrm{m/s}$ for *Pseudomonas putida* [46]. The insets show a characteristic trajectory (spatial scale in μm) for the noise amplitude indicated by a black dot in the main figure. The trajectories represent a time windows of $\Delta t = 26\,\mathrm{min}$ (left) and $\Delta t = 3\,\mathrm{s}$ (right). The red shaded regions indicate noise amplitudes expected for myxobacteria, $D_\theta \in (0.002, 0.02)\,\mathrm{s}^{-1}$ [45, 47], and *Pseudomonas putida*, $D_\theta \in (0.2, 0.4)\,\mathrm{s}^{-1}$ [46], respectively.

maximizes the diffusivity if the run-time distribution is sufficiently narrow. This resonance effect can be understood as a matching of timescales of the rotational diffusion and the mean time between two reversals.

We conclude by discussing the potential relevance of this resonance effect in microbiological systems by estimating and comparing the order of magnitude of relevant time and length scales from experimental data obtained in previous works [17,24,45–47]. As an example, we consider two bacterial species: *Myxococcus xanthus* and *Pseudomonas putida*[+], both showing directional reversals [17, 24, 45–47]. The results are summarized

[+] We note that *Pseudomonas putida* was shown to exhibit a more complex motion pattern than considered in this work: forward and backward motion occur with different speeds [24]. Here, we

Table 2. Summary of estimated characteristic parameter values.

Myxococcus xanthus	*Pseudomonas putida*
$v_0 \approx 0.1\,\mu$m/s [45]	$v_0 \approx 40\,\mu$m/s [46]
$D_\theta \in (0.002, 0.02)\,\mathrm{s}^{-1}$ [45, 47]	$D_\theta \in (0.2, 0.4)\,\mathrm{s}^{-1}$ [46]
$\langle t \rangle \approx 8.6\,$min [17]	$\langle t \rangle \approx 1.5\,$s [24]

in Fig. 9. We first estimated the coefficients $\{M, \kappa\}$ from the experimentally observed run-time distributions $\varphi(t)$ via the relations of these model parameters to the mean $\langle t \rangle$ and the variance $\sigma^2 = \langle t^2 \rangle - \langle t \rangle^2$ of the run-time distribtion (cf. section 3.1):

$$\kappa = \frac{1}{\left[\langle t \rangle \sigma^2\right]^{1/3}}\,, \quad M = \frac{\langle t \rangle}{\left[\langle t \rangle \sigma^2\right]^{1/3}}\,. \tag{5.1}$$

Besides the characteristics of the reversal process, we estimated characteristic speeds: $v_0 \approx 0.1\,\mu$m/s for myxobacteria [45] and $v_0 \approx 40\,\mu$m/s for *Pseudomonas putida* [46]. Knowing the characteristic speed v_0, the order of magnitude of the rotational noise D_θ can be estimated from the persistence of trajectories as provided in [47], or from direct measurements of the orientational correlation function [46]. However, we expect the persistence of trajectories and, consequently, the angular noise to be highly dependent on the environmental conditions and therefore do only consider rough estimates summarized in Tab. 2.

We find that the clock model provides an excellent fit to the run-time distributions for myxobacteria and *Pseudomonas putida*, even though the characteristic time scales of the two species differ by one order of magnitude, as illustrated in Fig. 9. Apparently, the reversal processes are not Poisson processes, since we obtain $M > 1$ in both cases. Furthermore, we find that an optimal rotational noise amplitude can exist indeed in the case of myxobacteria, which is not the case for *Pseudomonas putida*. The shape of trajectories in Fig. 9 suggest that the diffusion of *Pseudomonas putida* is dominated by reversal events whereas, in contrast, the timescales of rotational diffusion and reversal coincide roughly for myxobacteria. Our analysis suggests that the coincidence of rotational noise and reversal frequency leads to an optimal (maximal) diffusion. It will be very interesting to check experimentally whether the "natural parameters" of other microbiological systems were evolutionary tuned in such a way that microorganisms are best adapted to their environment in the sense that their diffusivity is optimal – a prerequisite for an optimal food search strategy.

A further aspect where the described model for reversing bacteria may become important is the modeling of collective behaviors like rippling, clustering and other forms of collective motion of bacteria. Earlier studies on myxobacterial rippling [27, 48] compared simulation results with experimental data [27, 49] based on the reversal time statistics of labeled bacteria in colonies assuming identical cell behaviors. The presented

do not intend to describe these bacteria in full detail but use the illustrative example to estimate the order of magnitude of characteristic quantities such as the diffusion coefficient.

model, in contrast, allows for the modeling of the variability of individual cells that is expressed in the run-time distributions displayed in Fig. 9.

Acknowledgement

RG and MB gratefully acknowledge the support by the German Research Foundation via Research Training Group 1558. FP acknowledges support by the Agence nationale de la recherche via JCJC project "BactPhys" and by the Fédération W. Döblin (CNRS) via AxePhysBio project "The Physics of Bacterial Invasion".

References

[1] Toner J, Tu Y and Ramaswamy S 2005 *Ann. Phys.* **318** 170–244
[2] Romanczuk P, Bär M, Ebeling W, Lindner B and Schimansky-Geier L 2012 *Eur. Phys. J. - Spec. Top.* **202** 1–162
[3] Marchetti M C, Joanny J F, Ramaswamy S, Liverpool T B, Prost J, Rao M and Simha R A 2013 *Rev. Mod. Phys.* **85** 1143–1189
[4] Menzel A M 2015 *Phys. Rep.* **554** 1–45
[5] Paxton W F, Kistler K C, Olmeda C C, Sen A, Angelo S K S, Cao Y, Mallouk T E, Lammert P E and Crespi V H 2004 *J. Am. Chem. Soc.* **126** 13424–13431
[6] Palacci J, Abécassis B, Cottin-Bizonne C, Ybert C and Bocquet L 2010 *Phys. Rev. Lett.* **104**(13) 138302
[7] Bricard A, Caussin J B, Desreumaux N, Dauchot O and Bartolo D 2013 *Nature* **503** 95–98
[8] Bricard A, Caussin J B, Das D, Savoie C, Chikkadi V, Shitara K, Chepizhko O, Peruani F, Saintillan D and Bartolo D 2015 *Nat. Commun.* **6** 7470
[9] Vicsek T and Zafeiris A 2012 *Phys. Rep.* **517** 71–140
[10] Ginelli F, Peruani F, Pillot M H, Chaté H, Theraulaz G and Bon R 2015 *Proc. Natl. Acad. Sci. USA* **112** 12729–12734
[11] Toulet S, Gautrais J, Bon R and Peruani F 2015 *PLoS ONE* **10** e0140188
[12] Peruani F, Starruß J, Jakovljevic V, Søgaard-Andersen L, Deutsch A and Bär M 2012 *Phys. Rev. Lett.* **108**(9) 098102
[13] Peruani F, Deutsch A and Bär M 2006 *Phys. Rev. E* **74**(3) 030904
[14] Wensink H H, Dunkel J, Heidenreich S, Drescher K, Goldstein R E, Löwen H and Yeomans J M 2012 *Proc. Natl. Acad. Sci. USA* **109** 14308–14313
[15] Dunkel J, Heidenreich S, Drescher K, Wensink H H, Bär M and Goldstein R E 2013 *Phys. Rev. Lett.* **110**(22) 228102
[16] Großmann R, Romanczuk P, Bär M and Schimansky-Geier L 2014 *Phys. Rev. Lett.* **113**(25) 258104
[17] Wu Y, Kaiser A D, Jiang Y and Alber M S 2009 *Proc. Natl. Acad. Sci. USA* **106** 1222–1227
[18] Thutupalli S, Sun M, Bunyak F, Palaniappan K and Shaevitz J W 2015 *J. R. Soc. Interface* **12**
[19] Johansen J E, Pinhassi J, Blackburn N, Zweifel U L and Hagström A 2002 *Aquat. Microb. Ecol.* **28** 229–237
[20] Barbara G M and Mitchell J G 2003 *FEMS Microbiol. Ecol.* **44** 79–87
[21] Be'er A, Strain S K, Hernández R A, Ben-Jacob E and Florin E L 2013 *J. Bacteriol.* **195** 2709–2717
[22] Duffy K J and Ford R M 1997 *J. Bacteriol.* **179** 1428–1430
[23] Davis M L, Mounteer L C, Stevens L K, Miller C D and Zhou A 2011 *J. Biosci. Bioeng.* **111** 605–611
[24] Theves M, Taktikos J, Zaburdaev V, Stark H and Beta C 2013 *Biophys. J.* **105** 1915–1924
[25] Raatz M, Hintsche M, Bahrs M, Theves M and Beta C 2015 *Eur. Phys. J. - Spec. Top.* **224** 1185–1198

[26] Börner U, Deutsch A, Reichenbach H and Bär M 2002 *Phys. Rev. Lett.* **89**(7) 078101
[27] Sliusarenko O, Neu J, Zusman D R and Øster G 2006 *Proc. Natl. Acad. Sci. USA* **103** 1534–1539
[28] Taylor B L and Koshland D 1974 *J. Bacteriol.* **119** 640–642
[29] Xie L, Altindal T, Chattopadhyay S and Wu X L 2011 *Proc. Natl. Acad. Sci. USA* **108** 2246–2251
[30] Stocker R 2011 *Proc. Natl. Acad. Sci. USA* **108** 2635–2636
[31] Taktikos J, Stark H and Zaburdaev V 2013 *PLoS One* **8** e81936
[32] Romanczuk P 2011 *Active motion and swarming: From individual to collective dynamics* vol 12 (Logos Verlag Berlin)
[33] Leonardy S, Bulyha I and Søgaard-Andersen L 2008 *Mol. BioSyst.* **4** 1009–1014
[34] Rashkov P, Schmitt B A, Søgaard-Andersen L, Lenz P and Dahlke S 2012 *B. Math. Biol.* **74** 2183–2203
[35] Romanczuk P and Schimansky-Geier L 2011 *Phys. Rev. Lett.* **106**(23) 230601
[36] Großmann R, Peruani F and Bär M 2015 *Eur. Phys. J. - Spec. Top.* **224** 1377–1394
[37] Schienbein M and Gruler H 1993 *B. Math. Biol.* **55** 585–608
[38] Mikhailov A and Meinköhn D 1997 Self-motion in physico-chemical systems far from thermal equilibrium *Stochastic Dynamics* (*Lecture Notes in Physics* vol 484) ed Schimansky-Geier L and Pöschel T (Springer Berlin Heidelberg) pp 334–345
[39] Taylor G I 1922 *P. Lond. Math. Soc.* **s2-20** 196–212
[40] Kubo R 1957 *J. Phys. Soc. Jpn.* **12** 570–586
[41] Doetsch G 1947 *Tabellen zur Laplace-Transformation und Anleitung zum Gebrauch* (*Die Grundlehren der mathematischen Wissenschaften in Einzeldarstellungen mit besonderer Berücksichtigung der Anwendungsgebiete* no 54) (Springer)
[42] Gardiner C 2010 *Stochastic Methods: A Handbook for the Natural and Social Sciences* Springer Series in Synergetics (Springer)
[43] Feller W 2008 *An introduction to probability theory and its applications* vol 2 (John Wiley & Sons)
[44] Godrèche C and Luck J 2001 *J. Stat. Phys.* **104** 489–524
[45] Sliusarenko O, Zusman D R and Øster G 2007 *J. Bacteriol.* **189** 611–619
[46] Theves M, Taktikos J, Zaburdaev V, Stark H and Beta C 2015 *Europhys. Lett.* **109** 28007
[47] Jelsbak L and Søgaard-Andersen L 2002 *Proc. Natl. Acad. Sci. USA* **99** 2032–2037
[48] Börner U, Deutsch A and Bär M 2006 *Phys. Biol.* **3** 138
[49] Welch R and Kaiser D 2001 *Proc. Natl. Acad. Sci. USA* **98** 14907–14912